DOI: http://dx.doi.org/10.12989/was.2012.15.4.331

Wind pressure on a solar updraft tower in a simulated stationary thunderstorm downburst

Xinping Zhou*[1,2], Fang Wang[1] and Chi Liu[1]

[1]*Department of Mechanics, School of Civil Engineering and Mechanics, Huazhong University of Science and Technology, Luoyu Road 1037, Wuhan, Hubei 430074, PR China*
[2]*Technical Center, Maanshan Iron and Steel Co. Ltd., Maanshan, Anhui 243000, PR China*

(Received May 19, 2011, Revised August 26, 2011, Accepted September 2, 2011)

Abstract. Thunderstorm downbursts are responsible for numerous structural failures around the world. The wind characteristics in thunderstorm downbursts containing vortex rings differ with those in 'traditional' boundary layer winds (*BLW*). This paper initially performs an unsteady-state simulation of the flow structure in a downburst (modelled as a impinging jet with its diameter being D_{jet}) using a computational fluid dynamics (*CFD*) method, and then analyses the pressure distribution on a solar updraft tower (*SUT*) in the downburst. The pressure field shows agreement with other previous studies. An additional pair of low-pressure region and high-pressure region is observed due to a second vortex ring, besides a foregoing pair caused by a primary vortex ring. The evolutions of pressure coefficients at five orientations of two representative heights of the *SUT* in the downburst with time are investigated. Results show that pressure distribution changes over a wide range when the vortices are close to the *SUT*. Furthermore, the fluctuations of external static pressure distribution for the *SUT* case 1 (i.e., radial distance from a location to jet center x=D_{jet}) with height are more intense due to the down striking of the vortex flow compared to those for the *SUT* case 2 (x=2D_{jet}). The static wind loads at heights z/H higher than 0.3 will be negligible when the vortex ring is far away from the *SUT*. The inverted wind load cases will occur when vortex is passing through the *SUT* except on the side faces. This can induce complex dynamic response of the *SUT*.

Keywords: wind pressure; solar updraft tower; thunderstorm downburst; vortex

1. Introduction

Thunderstorm downbursts, realized as an extreme weather, induced numerous structural failures around the world. Fujita (1985) defined a downburst as a strong downdraft which leads to outburst of damaging winds on or near the ground. The wind structure is different from that of low-speed boundary layer winds (*BLW*) which has an increasing velocity from the ground. The horizontal velocity of thunderstorm wind on the ground initially increases to its peak near the ground and then decreases with height. The wind loads on structures especially long-span bridges and high structures in a downdraft are more complex. However, the current design wind loads for structures are based on the low-speed *BLW*. It has been recorded that, 2/3 of high-intensity wind events in North Eastern United States involving damaging effect on buildings and other structures are associated with the

* Corresponding author, Dr. Xinping Zhou, E-mail, xpzhou08@mail.hust.edu.cn

thunderstorms (Kim and Hangan 2007). Outside of hurricane regions, up to 75% of the peak gust wind speeds occurred during thunderstorms in the USA (Sengupta and Sarkar 2008). Thunderstorms are responsible for about 90% of the 94 records of Australian transmission line failures due to high-intensity winds (Hawes and Dempsey 1993).

The simulated velocity profile by using the impinging jet model showed to be more uniform to mean characteristics of the full-scale downbursts from the Joint Airport Weather Studies (*JAWS*) Project (Hjelmfelt 1988). Since that, several research groups studied the characteristics of the microburst jets based on experimental measurements, physical modelings and numerical simulations. Most of the previous physical modelings and numerical simulations incorporated either a stationary (Sengupta and Sarkar 2008, Holmes and Oliver 2000, Wood *et al*. 2001) or a translating impinging wall jet (Chay and Letchford 2002), or an impulsively started one (Kim and Hangan 2007, Mason *et al*. 2005, Mason *et al*. 2009a). Lin *et al*. (2007) used a slot jet with an actuated gate to simulate the non-stationary behavior of downburst. Mason *et al*. (2009b) used an axisymmetric, dry, non-hydrostatic numerical sub-cloud model, where some form of forcing typically microphysical is imposed at an elevated region of the domain, to simulate the characteristics of an intense stationary downburst. A simplified imposed cooling source was used to force the downdraft in place of the computationally expensive microphysics models typically used. The outflow velocity field is showed comparable with *JAWS* data and impinging jet models. In the previous work, the computational fluid dynamics (*CFD)* modelling technology has been found to be a reliable and realizable method validated by experimental measurements. Selvam and Holmes (1992), and later Wood *et al*. (2001) used a two-dimensional model to investigate the wind velocity profiles of downburst winds over a hill. Kim and Hangan (2007) used a Reynolds stress model (*RSM*) to investigate the characteristics of downburst modeled as a two-dimensional axisymmetric flow about the vertical axis. Three-dimensional downburst wind fields were simulated by Mason *et al*. (2010) by solving equations using the unsteady Reynolds Averaged Navier–Stokes (*URANS*) approximation, and closing with the Scale Adaptive Simulation (*SAS*) turbulence model, which is the improved version of URANS method providing the large eddy simulation (*LES*)-like behavior in unsteady regions of the flow field for a sufficiently fine mesh.

Solar updraft tower (*SUT*) power technology is a promising clean technology for large-scale

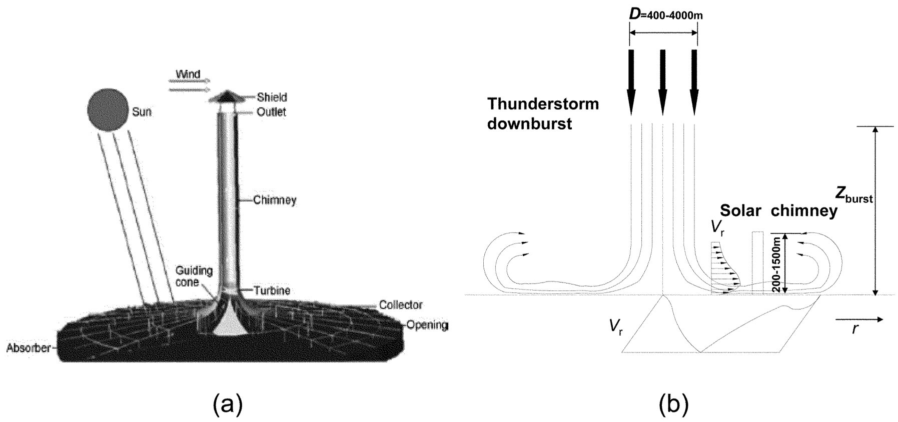

Fig. 1 (a) Schematic diagram of *SUT* power system (Zhou *et al*. 2008) and (b) schematic diagram of thunderstorm downburst and its potential impact on high *SUT*

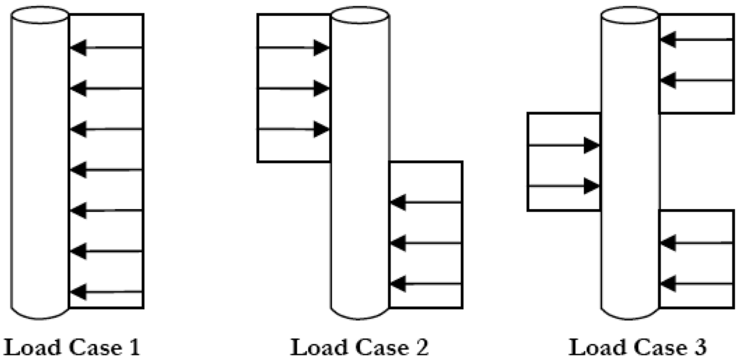

Fig. 2 Three wind load cases showing direction, not wind speed, which varies over height (Rousseau 2005, Harte *et al*. 2007)

power generation (Schlaich 1995, Zhou *et al*. 2009), which was tested with a 50 kW Manzanares prototype plant in the early 1980s (Haaf 1984). The *SUT* power plant combines three components: a solar collector, a *SUT* situated in the center of the collector, and turbine generators. It works on the principle that the turbines are driven by airflow produced by buoyancy derived from hot air heated by the collector. The conversion efficiency of this type of plant is low as determined by its thermal performance. *SUT* works as the heat engine of the system. Higher *SUT* can therefore help to increase the power plant's conversion efficiency and then lead to a reduction in the energy cost. For commercial *SUT* power plants producing energy economically, not only is a large collector area necessary for collecting solar energy, but also a high and large *SUT* is required to house a big turbine or several small turbines in a plane (Zhou *et al*. 2010) and to obtain a large driving force (Schlaich 1995). Recently, the Australian government decided to support the construction of a 200 MW *SUT* power generating plant prototype with a 1 km *SUT* in Mildura, Australia (Zhou *et al*. 2010). *SUT* is usually designed as a high rigid thin-walled hollow structure whose design height usually changes from 200 m to 1500 m (Schlaich 1999, von Backström *et al*. 2008). The design of high *SUT* is governed by wind loads. Kim *et al*. (2007) compared the base shear force and base moments of tall building subjected to downburst and those subjected to *BLW*, with matched 10-meter wind velocity. It is concluded that downbursts larger than about 2000 m in diameter become governing design wind loads instead of *BLW* for tall buildings. Mason *et al*. (2010) also drew a similar conclusion. Although, Rousseau (2005) presented the possibility of inverted wind load cases (Fig. 2) in a thunderstorm and simply analyzed the characteristics of dynamic response of high *SUT* exposed to the three wind load cases by taking a reference *SUT* 1500 m high and 160 m in internal diameter as an example. The results showed that the uni-directional wind (Load case 1) dominates at low frequency, while the higher vibrational modes are excited by inverted load cases 2 and 3 (Rousseau 2005, Harte *et al*. 2007). In reality, the inverted wind load cases for the high rotational *SUT* structure are more complex than the simple diagram as shown in Fig. 2. It is significant to study the wind pressure distribution on high *SUT*, which will lay the foundation to analyses of the complex dynamic responses of the *SUT*.

In this paper, we use the *CFD* model validated by experimental measurement to simulate the air flow in a thunderstorm downburst and analyze the pressure distribution on the *SUT* surface by taking a 1000 m high *SUT* case as an example.

2. Numerical simulation

Sengupta and Sarkar (2008) used five available turbulence models of a commercially available *CFD* software Fluent (i.e., Standard, *RNG*, and Realizable *k*–epsilon models, shear–stress transport *k*–omega model, -*RSM* and *LES*) to simulate the flow of thunderstorm downburst and the results do not differ much with measurements. In our paper, the flow of a stationary downburst is simulated using Fluent (version 6.3.26) (2006). Considering vortex dynamics of full scale downburst, *LES* is chosen. In the Fluent *LES* model, three models (i.e., the dynamic Smagorinsky-Lilly model, *WALE* model, and Kinetic-Energy Transport model) are available to calculate the eddy viscosity. In the work of Sengupta and Sarkar (2008), the use of the dynamic Smagorinsky-Lilly model of *LES* model produced good results compared to the measurements and other turbulence models. In our paper, the dynamic Smagorinsky-Lilly model of *LES* model is therefore used. The central difference scheme is used, and the Pressure-Implicit with Splitting of Operators (*PISO*) algorithm is used for the pressure correction for the unsteady-state simulation. Detailed information about the *LES* model can be found in the User's Guide of Fluent (2006).

The computational cost related to the investigation of a three-dimensional model of large computational domain is high. This determines a partial model is more effective for the simulation study. In order to ensure that the air flow around the *SUT* and the boundaries of the partial model do not affect each other incorrectly when simulating the air flow in the computational domain, a very small partial model is not suitable. A quarter of the three-dimensional model is therefore used in the *CFD* model with schematic diagram of the computational domain shown in Fig. 3, in which the height and radius are set 4 times and 6 times as large as the jet diameter (D_{jet}). Two cases are selected to demonstrate the influence of *SUT* locations on its wind pressure distribution, i.e., case 1,

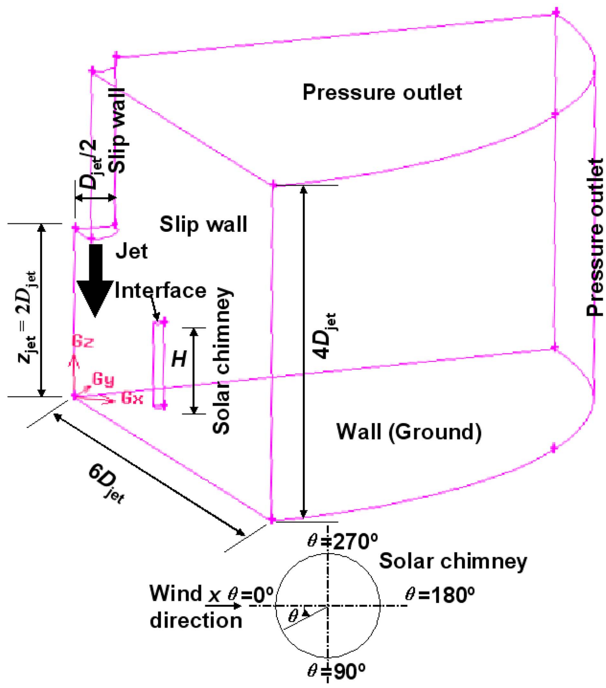

Fig. 3 Schematic diagram of computational domain (case 1)

(radial distance from a location to jet center x = D_{jet}), and case 2 (x = 2 D_{jet}). By taking a jet 1000 m in diameter with height from the ground z_{jet}=2 D_{jet} and its inlet velocity set at 40 m/s corresponding to Reynolds number of 2.7×10^9 as an example, we perform the simulation of downburst wind. A Cartesian coordinate system with an origin at the ground on the centerline of the jet is employed, with z measured away from the ground, and in the domain, being symmetric about y axis, positive x is downstream.

The pressure coefficients on the *SUT* surface can be calculated by

$$C_p = \frac{P_i - P_\infty}{\overline{\frac{1}{2}\rho V_{ref}^2}} \tag{1}$$

where, P_∞ is the ambient static pressure, P_i is the static pressure on the *SUT* surface, and $\overline{\frac{1}{2}\rho V_{ref}^2}$ is the mean dynamic pressure at the reference location which is chosen at the inlet of impinging jet in this work.

3. Results and discussion

3.1 Unsteady-state downburst flow

Unsteady-state simulations are conducted in order to better understand the dynamics of the flow of full-scale thunderstorm downburst where time is non-dimensionalized by the jet velocity (V_{jet}) and the jet outlet diameter as

$$T = tV_{jet} / D_{jet} \tag{2}$$

To ensure that the calculated results are not influenced by grid number, grid independency of the *LES* simulations is performed. Three different grid sizes, namely, coarse (2 million cells), medium (3 million cells), and fine (4 million cells), are tested. The results at $x = 1\ D_{jet}$ and 2 D_{jet} at $T = 12$ with the three grid sizes and the full-scale data of *JAWS* downburst are compared. The comparison shows the results for the medium and the fine grid sizes do not differ much. All the results are therefore based on the medium grid in this paper. Furthermore, the flow fields of downburst outflow near the ground for $x/D_{jet} = 1$ at $T = 12$ and 36.4 when downburst is relatively steady based on the medium grid size are comparable with full-scale data of *JAWS* downburst (Hjelmfelt 1988, Chay and Letchford 2002) and empirical model presented by Peng (2008), as shown in Fig. 4. In the figure, the velocity is non-dimensionalized by the maximum of a vertical profile of horizontal velocity V_{max} at a height z_{max}, and the height is also non-dimensionalized by z_{max}, and only the heights higher than z_{max} are presented in order to illustrate the difference clearly. The vertical profile of horizontal velocity at a given radius was given by Peng (2008) as

$$\frac{V}{V_{max}} = 1.4 \cdot (exp(-0.95z/z_{0.5V_{max}}) - exp(-11.4z/z_{0.5V_{max}})) \tag{3}$$

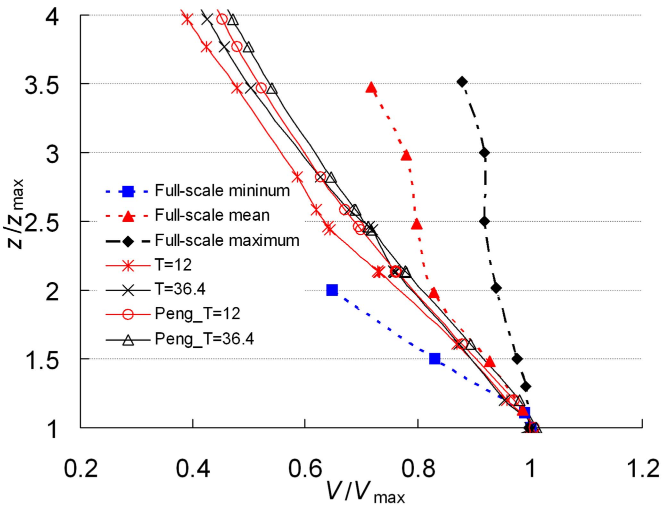

Fig. 4 Comparisons of results using our model and full-scale data of *JAWS* downburst and Peng's empirical model (2008)

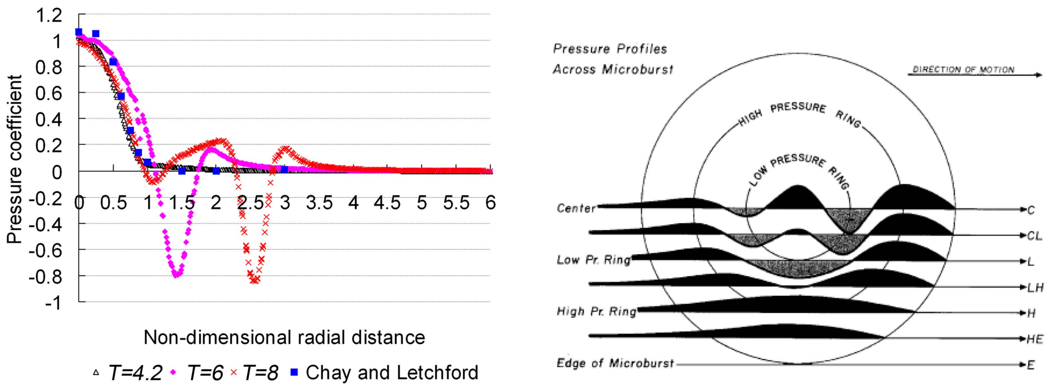

(a) (b)

Fig. 5 Radial distribution of static pressure near the ground (a) exposed to a stationary downburst at different time of 4.2, 6, and 8 as compared to Chay and Letchford (2002) and (b) a reference pressure field of a downburst (Fujita 1985)

where $z_{0.5V_{max}}$ is the height where the horizontal velocity is equal to half of V_{max}, which is higher than z_{max}. Eq. (3) was validated with the published results for other models in Peng's thesis (2008).

Fig. 5(a) shows the radial distribution of static pressure near the ground (at 0.1 m height) at T=4.2, 6, and 8. The surface pressures are finally compared with the pressure profile measured in an experimental quasi-steady impinging jet by Chay and Letchford (2002), and the classical surface pressure profile (Fig. 5(b)) due to the passage of a horizontal vortex, which was hypothesized by Fujita (1985). In the figure, a high-pressure core is produced in the center ground due to stagnation. No other high-pressure or low-pressure regions are formed at $T=4.2$ when the vortex does not reach the ground. At this time, the pressure field is shown uniform with the measurements by Clay and Letchford (2002). At $T = 6$, a negative low-pressure and the next less-intense high-pressure regions are formed in succession because the flow horizontal velocity near the ground initially increases to a peak around a primary vortex ring (the results of the strong Kelvin–Helmholtz instability (Kim and Hangan 2007)) and then decreases. Finally, the pressure is equal to ambient pressure at far radial distance. This phenomenon was also well reported by Fujita (1985) (Fig. 5(b)). This pair of low-pressure and foregoing high-pressure regions moves along due to the motion of the primary vortex following downburst. At $T = 8$, an additional pair of low-pressure region and high-pressure regions is produced due to a second vortex ring (the results of the initial quasi-periodic Kelvin–Helmholtz instability (Kim and Hangan 2007)). Compared to the first pair of low-pressure region and high-pressure regions, the low-pressure region is lower in intensity, and the cover area of the high-pressure region is larger. The static pressure is reduced by about 2 kPa from the center to the first low-pressure region. For steady-state flow, the negative pressure is not produced, as observed by Fujita (1985), and Chay and Letchford (2002) because the vortex rings are transient.

3.2 Unsteady-state downburst flow for the two SUT cases

We study the characteristics of the pressure distribution on the *SUT* external surface by analyzing unsteady-state downburst flow for two *SUT* cases in the thunderstorm respectively.

In order to analyze the static pressure at different heights exposed to downburst, two representative heights z/H of 0.05 and 0.6 are selected according to the vertical profiles of downburst winds, because the measurements by Chay and Letchford (2002) showed maximum horizontal velocity occurs around the height $z_{max}/H = 0.05$ and is very low at higher height (e.g., $z/H = 0.6$). Fig. 6 presents the evolution of the pressure coefficients at the two representative heights at five θ (θ is defined as the horizontal angle measured from the windward meridian, i.e., from the front stagnation point) angles of 0°, 45°, 90°, 135°, and 180° with time for *SUT* cases 1 and 2.

As seen from Fig. 6, for *SUT* cases 1 and 2, the static pressures are far away from 0 during the time period when the vortices are passing through the *SUT*. The variations of the values with time are basically uniform for θ angles of 45°, 90°, and 135°, and the largest-amplitude variation occurrs

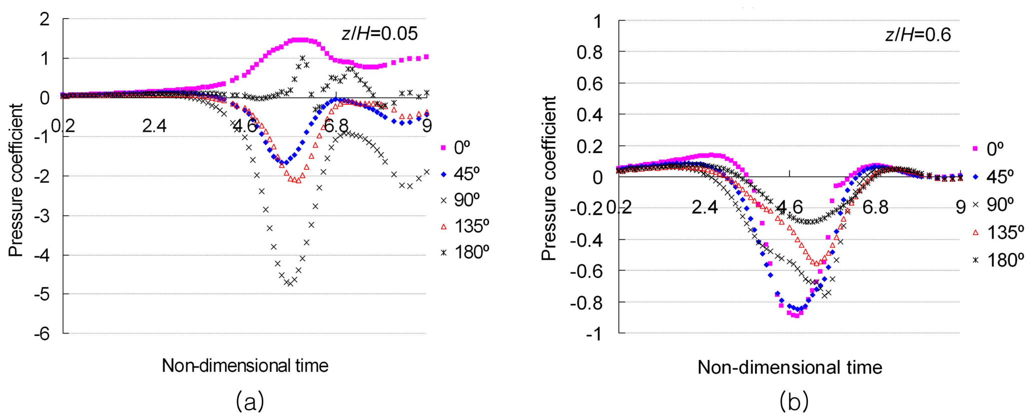

Fig. 6 Evolution of the pressure coefficients at two heights z/H of 0.05 and 0.6 at five θ angles of 0°, 45°, 90°, 135°, and 180° with time T from 0.2 to 9 for *SUT* cases 1 and time T from 0.2 to 10.8 for *SUT* case 2 (a) at height z/H 0f 0.05 of *SUT* case 1, (b) at height z/H 0f 0.6 of *SUT* case 1, (c) at height z/H 0f 0.05 of *SUT* case 2 and (d) at height z/H 0f 0.6 of *SUT* case 2

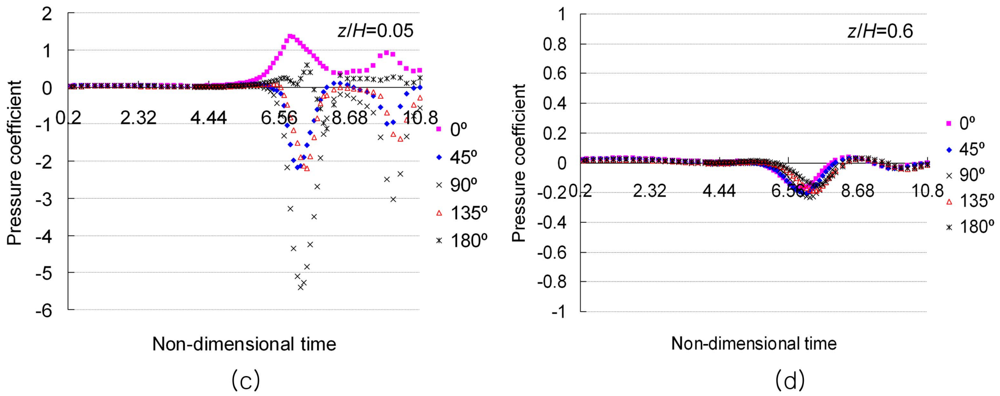

Fig. 6 Continued

at $\theta = 90°$. During the time, for the *SUT* case 1, at the height z/H of 0.05, the pressures at $\theta = 0^o$ are positive and most pressures at $\theta = 180^o$ are positive due to rotation of vortex flow, and the pressures at θ angles of 45º, 135º, and 90º are negative, reaching their minimum values. At the height z/H of 0.05, the maximum pressure coefficient of 1.45 for $\theta = 0^o$ at $T = 5.8$, and the minimum value of -4.73 for $\theta = 90^o$ at $T = 5.7$ are higher than the corresponding maximum value of 1.35 for $\theta = 0^o$ at $T = 6.9$ and minimum value of –5.41 for $\theta = 90^o$ at $T = 7.2$ for the *SUT* case 2.

Chay and Letchford (2002) tested the pressure along the windward, top, leeward faces and side face of a cube 30 mm in length ($z/D_{jet} = 0.059$) for different x/D_{jet} positions subjected to a simulated quasi-steady downburst jet 0.51 m in diameter. An extensive flat test surface was positioned 1.7 D_{jet} above the outlet of the impinging jet. Mason *et al*. (2009a) performed similar work for the cube subjected to a pulsed impinging jet instead of a quasi-steady impinging jet. The pressure at x/D_{jet} = 1 against a developed centre line coordinate normalized by the height of the cube subjected to the two different impinging jets were tested. Fig. 7 shows mean pressure coefficients along windward (0-1) and leeward (2-3) faces of the cube subjected to a quasi-steady jet, and averaged maximum pressure coefficients along windward, leeward, and side (3-4) faces of the cube subjected to a pulsed impinging jet. Peak pressure was defined as the average of the peak recorded pressure induced by the primary vortex at each discrete tap for all the individual testing runs (Mason *et al*. 2009a). The highlighted position z/D_{jet} is equal to about 0.05. The authors believe that the fact that the peak occurred between Point 0 to Point 1 is because z_{max}/D_{jet} for maximum velocity in the vertical direction is below 0.05. By comparing results from Figs. 6 and 7, in fact, the difference of the results for cylindrical *SUT* using current model and the cube are in part due to different shapes of the structures. Due to the vortex ring, the pressure peak is about 1.5 times as that subjected to the quasi-steady downdraft, and both of them are much less than the extremely high value (which is equal to about 3 at z/D_{jet} = 0.05) subjected to the pulsed downdraft resulted from the pulsing of impinging jet. Mason *et al*. (2009a) believed this is in part due to a funneling of air occurring as the experimental aperture is being opened. When outflow flows from Point 3 to Point 4, the (negative) pressure increases. The trend varying from Point 3 to Point 4, is similar to the *SUT* for θ varying from 0º to 45º to 90º to 135º and to 180º as shown in Fig. 6. However, the peak suction for the side surface of the *SUT* is a little larger than the average of the 6 testing points at the middle line at the height $z/D_{jet} = 0.03$. Their difference can mainly be attributed to different shapes of the two structures. Furthermore, unlike the previous studies, when the present vortices are passing through

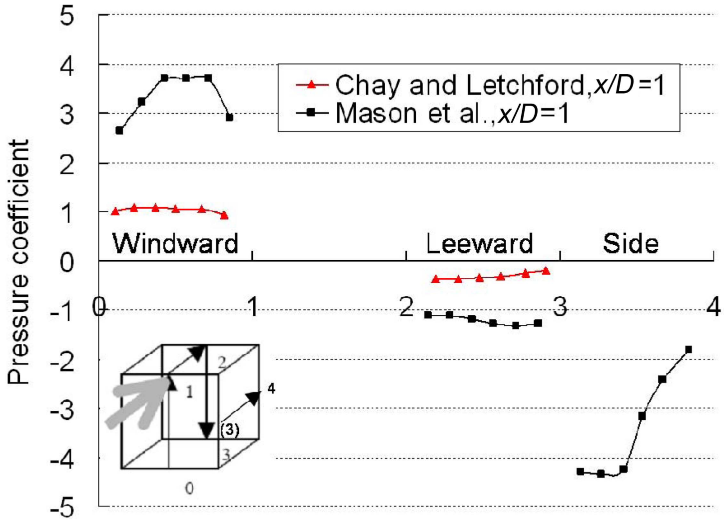

Fig. 7 Mean pressure coefficients along windward (0-1), and leeward (2-3) faces, of the cube subjected a quasi-steady jet, and averaged maximum pressure coefficients along windward, leeward faces, and side (3-4) faces of the cube subjected a pulsed impinging jet for x/D_{jet} = 1

the *SUT*, the pressure at θ=180º reaches a positive peak while that at θ =135º reaches a negative peak. This is because rolling of air induced by the present vortices has an influence on the wake zone.

When the vortices are passing through the *SUT*, at the height z/H = 0.6, the static pressures at all the θ angles become negative influenced by low-pressure vortex, and the minimum static pressure coefficient for the *SUT* case 1 is lower at –0.89 due to the effect of down striking of vortex flow compared to that value of –0.23 for the *SUT* case 2. The variations of the pressure coefficients with time are basically uniform for all the five θ angles. Furthermore, the variations of the values with time at all the five θ angles of height z/H = 0.6 are more uniform than those for the height z/H = 0.05. The negative-pressure regions occur when T varies between 2.6 and 7.2 for the *SUT* case 1, and between 5.6 and 8.4 for the *SUT* case 2. Finally, the pressure coefficients keep steadier after T = 6.8 except a lower-intensity low-pressure region due to the second vortex for the *SUT* case 1 and after T=8.4 for the SUT case 2. It is also found that the fluctuation of static pressure for the upper *SUT* case 1 is more intense than the upper *SUT* case 2 due to the down striking of the vortex flow.

Figs. 8(a) and (b) show the variation of static pressure with distance in the along-wind direction and the across-wind direction at two reference heights z/H of 0.05 and 0.6, respectively, in the computational domain, for the *SUT* case 1 at T = 4. As expected, by excluding the static pressure on the *SUT* inner surface, the static pressure on the *SUT* outer surface is just the lowest in the domain in the across-wind direction. In the along-wind direction, the pressure decreases along the radius from the high pressure center to a low value around the vortex, increases to a value on the SUT outer surface at θ =0º, and gradually varies from the pressure on the *SUT* outer surface at θ = 180º to approximately 0 at the height x/D_{jet} = 2. The static pressure coefficient on the *SUT* inner surface at the heights z/H of 0.05 and 0.6 is close to 0 and –0.1, respectively. The static pressures at the inner and outer surface of the SUT at the height z/H of 0.05 are higher than the values at the height z/H = 0.6 because the downburst flow influences the inflow and outflow velocity at the

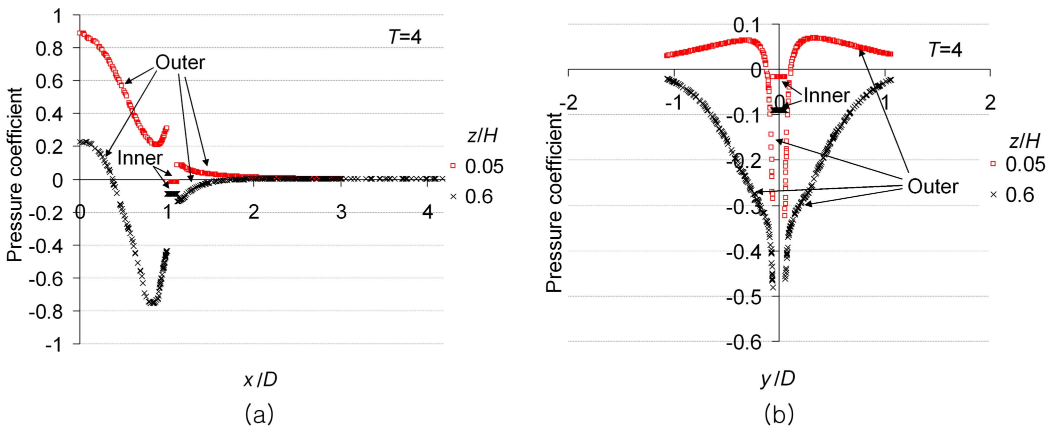

Fig. 8 Variation of static pressure at heights z/H = 0.05 and 0.6 in the computational domain for *SUT* case 1 with distance (a) in the along-wind direction and (b) in the across-wind direction

height z/H = 0.6 much more than at the height z/H =0.05.

Fig. 9 shows the variation of static pressure on the *SUT* case 1 outer surface at θ angles of 0°, 90°, and 180° with heights at T = 0.7, 4, 5.2, 6, and 12. At T = 0.7, the static pressure gradually increases with heights z/H from 0 to 1. When the vortex is close to the *SUT*, e.g., the time period between 4 and 6, the static pressures at the three θ angles fluctuate largely with the heights z/H from 0 to 1. At T = 12, the static pressure at the height z/H higher than 0.3 is approximately equal to 0.

At the time (e.g., T = 0.7) before the downdraft reaches the *SUT*, the wind forces (suction) at θ = 0°, 90°, and 180° is straightly positive. This is influenced by the high pressure core. Apart from the time before the downdraft reaches the *SUT* (e.g., T = 4, 5.2, 6, and 12), the pressure at θ = 90° keeping negative as expected. At T=4, the pressure at θ = 0° starts to become negative when z/H is higher than 0.46, and the pressure at θ = 180° becomes negative when z/H is higher than 0.36. At T = 6, the pressure at θ = 0° becomes negative when z/H is higher than 0.37 and is between –0.1 and 0 when z/H is higher than 0.51, and the pressure at θ = 180° becomes negative when z/H is higher than 0.21. At T = 12, the pressure is kept to be close to 0 when z/H is higher than 0.3, and the pressure is positive apart from z/H between 0.19 and 0.27 where the minimum negative value is –0.16. This shows that the direction of wind force keeps steady after the passage of the vortex ring. The inverted wind load cases (Fig. 2) are important when the vortex is passing through the *SUT* except on the side faces. This can induce complex dynamic response of the *SUT* (Rousseau 2005, Harte *et al*. 2007). Also, the complex distribution of wind force on the *SUT* will be helpful for design of structural stiffnesses.

4. Conclusions

This paper describes the results of an unsteady-state study of pressure distribution on a *SUT* exposed to a thunderstorm downburst by using the *LES* in the commercial *CFD* code Fluent validated by experimental measurements (Sengupta and Sarkar 2008). The evolution of pressure field with time shows that the results obtained are related to those of earlier studies. A high-pressure

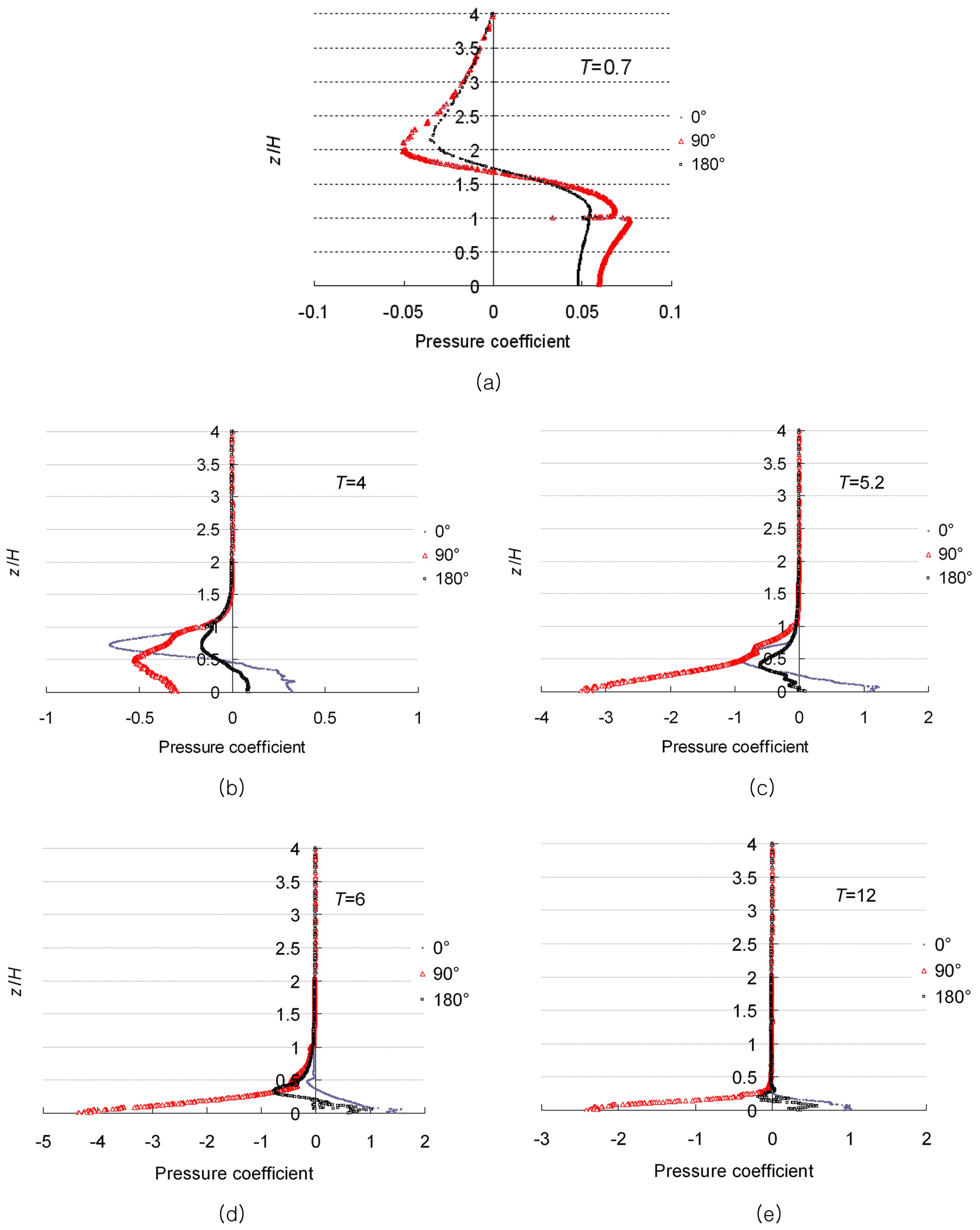

Fig. 9 Variation of static pressure on *SUT* case 1 outer surface at θ angles of 0^o, 90^o, and 180^o with heights at time (a) T = 0.7, (b) T = 4, (c) T = 5.2, (d) T = 6 and (e) T = 12

core is seen to be produced in the center ground due to stagnation and primary and second vortex rings are seen to form in tandem. A low-pressure and the next less-intense high-pressure regions are formed in succession because the velocity of flow near the ground initially increases to the peak horizontal velocity around the primary vortex ring and then decreases radially. In addition, an extra pair of low-pressure and high-pressure regions is observed due to the second vortex ring at a later time. The analyses show that the static pressure distribution on the *SUT* external surface fluctuates largely with time especially when the vortices are passing through the *SUT* surface, and that static wind loads at heights z/H higher than 0.3 will be negligible when the vortex ring is far away from the *SUT*. Furthermore, due to the down striking of the vortex flow, the fluctuation of external static pressure distribution for the *SUT* case 1 is far larger than for the *SUT* case 2. This can induce complex dynamic response of the *SUT*. This work will set a foundation for further investigation on dynamic response of high *SUT* exposed to downburst.

Acknowledgements

This research has been supported by the National Natural Science Foundation of China (No. 50908094), the Ph. D. Programs Foundation of Ministry of Education of China (No. 20100142120071), the Natural Science Foundation of Hubei Province (No. 2010CDB02204), and the Fundamental Research Fund for the Central Universities (No. 2012QN022)

References

Chay, M.T., Albermani, F. and Wilson, R. (2006), "Numerical and analytical simulation of downbursts wind loads", *Eng. Struct.*, **28**(2), 240-254.

Chay, M.T. and Letchford, C.W. (2002), "Pressure distributions on a cube in a simulated thunderstorm downburst-Part A: Stationary downburst observations", *J. Wind Eng. Ind. Aerod.*, **90**(7), 711-732.

Fluent 6.3.26 (2006), User's Guide, Fluent Inc., Lebanon, New Hampshire.

Fujita, T.T. (1985), *Downburst: Microburst and macroburst*, University of Chicago Press, Chicago, IL.

Haaf, W. (1984), "Solar chimneys. Part II: preliminary test results from the Manzanares pilot plant", *Int. J. Solar Energy*, **2**, 141-161.

Harte, R. and van Zijl, G.P.A.G. (2007), "Structural stability of concrete wind turbines and solar chimney towers exposed to dynamic wind action", *J. Wind Eng. Ind. Aerod.*, **95**(9-11), 1079-1096.

Hawes, H. and Dempsey, D. (1993), "Review of recent Australian transmission line failures due to high intensity winds", *Proceedings of the Task Force of High Intensity Winds on Transmission Lines*, Buenos Aires,Argentina.

Hjelmfelt, M.R. (1988), "Structure and life circle of microburst outflows observed in Colorado", *J. Appl. Meteorol.*, **27**(8), 900-927.

Holmes, J.D. and Oliver, S.E. (2000), "An empirical model of a downburst", *Eng. Struct.*, **22**(9), 1167-1172.

Kim, J. and Hangan, H. (2007), "Numerical simulations of impinging jets with application to downbursts", *J. Wind Eng. Ind. Aerod.*, **95**(4), 279-298.

Kim, J., Hangan, H. and Ho, T.C.E. (2007), "Downburst versus boundary layer induced wind loads for tall buildings", *Wind Struct.*, **10(5)**, 481-494.

Letchford, C.W. and Chay, M.T. (2002), "Pressure distributions on a cube in a simulated thunderstorm downburst-Part B: moving downburst observations", *J. Wind Eng. Ind. Aerod.*, **90**(7), 733-753.

Lin, W.E., Orf, L.G., Savory, E. and Novacco, C. (2007), "Proposed large–scale modelling of the transient features of a downburst", *Wind Struct.*, **10**(4), 315-346.

Mason, M.S., Fletcher, D.F. and Wood, G.S. (2010), "Numerical simulation of idealised three-dimensional downburst wind fields", *Eng. Struct*., **32**(11), 3558-3570.
Mason, M.S., James, D.L. and Letchford, C.W. (2009a), "Wind pressure measurements on a cube subjected to pulsed impinging jet flow", *Wind Struct*., **12**(1), 77-88
Mason, M.S., Letchford, C.W. and James, D.L. (2005), "Pulsed wall jet simulation of a stationary thunderstorm downburst, part A: physical structure and flow field characterization", *J. Wind Eng. Ind. Aerod*., **93**(7), 557-580.
Mason, M., Wood, G. and Fletcher, D. (2009b), "Numerical simulation of downburst winds", *J. Wind Eng. Ind. Aerod*., **97**(11-12), 523-539.
Peng, Z.W. (2008), *The numerical simulations of thunderstorm downbursts and its effect on low-flat structures*, Master Thesis, Zhejiang University, Hangzhou, China.
Rousseau, J.P. (2005), *Dynamic evaluation of the solar chimney*, MScEng–thesis, University of Stellenbosch, South Africa.
Schlaich, J. (1995), *The solar chimney: Electricity from the sun*, Edition Axel Menges, Stuttgart, Germany.
Schlaich, J. (1999), "*Tension structures for solar electricity generation*", *Eng. Struct*., **21**(8), 658-668.
Selvam, R.P. and Holmes, J.D. (1992), "Numerical simulations of thunderstorm downbursts", *J. Wind Eng. Ind. Aerod*., 41-44, 2817-2825.
Sengupta, A. and Sarkar, P.P. (2008), "Experimental measurement and numerical simulation of an impinging jet with application to thunderstorm microburst winds", *J. Wind Eng. Ind. Aerod*., **96**(3), 345-365.
Wood, G.S., Kwok, K.C.S., Motteram, N.A. and Fletcher, D.F. (2001), "Physical and numerical modelling of thunderstorm downbursts", *J. Wind Eng. Ind. Aerod*., **89**(6), 535-552.
Von Backström, T.W., Harte, R., Höffer, R., Krätzig, W.B., Kröger, D.G., Niemann, H.J. and van Zijl, G.P.A.G. (2008), *State and recent advances in research and design of solar chimney power plant technology*, VGB PowerTech Journal, PT07, 64.
Zhou, X.P., Wang, F. and Ochieng, R.M. (2010), "A review of solar chimney power technology", *Renew. Sust. Energ. Rev*., **14**(8), 2315-2338.
Zhou, X.P., Yang, J.K., Ochieng, R.M. and Xiao, B. (2009), "Numerical investigation of a plume from a power generating solar chimney in an atmospheric cross flow", *Atmos. Res*., **91**(1), 26-35.
Zhou, X.P., Yang, J.K., Xiao, B., Hou, G.X. and Shi, X.Y. (2008), "Special climate around a commercial solar chimney power plant", *J. Energ. Eng. - ASCE*, **134**(1), 6-14.

CC